The 8th European Congress on Computational Methods in Applied Sciences and Engineering
ECCOMAS Congress 2022
5-–9 June 2022, Oslo, Norway

IMPLEMENTATION OF CWENO SCHEMES FOR COMPRESSIBLE MULTICOMPONENT/MULTIPHASE FLOW USING INTERFACE CAPTURING MODELS

E.M. Adebayo[1], P. Tsoutsanis[1], K. W. Jenkins[1]

[1] School of Aerospace, Transport and Manufacturing
Cranfield University,
Cranfield MK43 0AL, United Kingdom,
email: e.adebayo@cranfield.ac.uk, panagiotis.tsoutsanis@cranfield.ac.uk,
k.w.jenkins@cranfield.ac.uk

Key words: Diffuse-Interface Models, High-Order Methods, Finite Volume, CWENO

Abstract. We present in this work shock-/interface-capturing numerical methods in the finite-volume central-weighted essentially non-oscillatory (CWENO) reconstruction scheme on unstructured grids for the simulation of multi-component or multiphase compressible flows. Using the five-equation interface capturing models of Allaire et al. and Kapila et al. in the open-source unstructured compressible flow solver `UCNS3D`, we will demonstrate the capabilities and robustness of the CWENO in capturing and resolving the material interface in multi-component/multiphase flows in the presence of strong gradients and material discontinuities, with oscillation free solutions and reduced numerical diffusion. To test our numerical methods, a simple one-dimensional test case and a more sophisticated 2d underwater test case with cavitation are considered. The numerical results of our study are compared with results from existing high-order methods. The results show that the CWENO is less dissipative without the spurious oscillations that typically develop at material boundaries and also gives a high-resolution description of the moving material interface with less artificial smearing than other high other schemes.

1 INTRODUCTION

Every compressible multiphase fluid has a characteristic interface which separates the phases. Unlike single-phase, compressible flows that involve only discontinuous waves, solving numerically multiphase compressible flow presents an additional discontinuity in the form of contact waves corresponding to the material interface between the fluids. Therefore, an additional numerical algorithm needs to be developed to treat the material interface of multiphase compressible flows aside from the Euler or Naiver-Stokes equation.

The conventional methods for treating the interface involve eliminating the numerical diffusion at the interface, which means the artificial mixing probable is also eliminated, often leading to inaccurately predicting the position of the material interface and the shock wave when the fluid features interact. These methods treat the interface as a sharp discontinuity (i.e. the physical shock structure is not resolved, making such methods referred to as the sharp interface

methods SIM (also interface -tracking methods in some literature). Such methods include the volume of fluid, level set, front tracking etc.

Another method is the diffused interface models (also referred to as the interface-capturing method). This method has a set of governing equations that are unconditionally hyperbolic systems of model that offer the advantages of utilizing the Godunov-type schemes and are very conservative, leading to accurate and efficient computations for internal energies and temperature at the interfaces [1]. Among the common DIM models are the Kapila's et al [2], Allaire's et al [3], Saurel's et al [4], Murrone's et al. [5], Romenski's et al. [6], which are all simplified models from the full seven-equation models of Baer-Nunziato's. The reader is referred to the work of Maltsev et al. [7] for an up to date comprehensive review of the DIM models.

For multiphase compressible flows, high-order schemes offer an advantage over lower-order schemes. They provide higher accuracy in the presence of shocks or discontinuities and higher resolution in the smooth region. In recent times, high order methods have been extensively used for compressible multiphase flow [8–10]. To provide non-oscillatory capabilities to a numerical framework of multiphase compressible flow, commonly used high order methods are the Discontinuous Galerkin DG method for finite element [11], WENO for finite difference method and WENO for finite volume methods [9, 12, 13]and also the MUSCL with the use of limiters. Finite difference WENO schemes are only applicable on uniform meshes or smooth curvilinear coordinates in multi-dimensional computation. This is a disadvantage of finite difference and the significant benefit of the finite volume WENO schemes over the finite difference WENO for compressible multiphase flow, even though Finite volume WENO schemes are computationally expensive and more complicated to code than the finite difference WENO.

The WENO is often used with an HLL or HLLC Harten-Lax-van Leer Contact HLLC approximate Riemann solver to upwind the fluxes. However, the discontinuous method for a finite element is less complicated for unstructured or distorted mesh [14]. The finite volume higher-order schemes such as WENO are more robust in the presence of strong shocks and computationally cheaper than the latter. Dumbser et al. [15] first used a WENO variation named CWENO on unstructured 2D and 3D meshes. CWENO one single set of linear weights and one set of valid nonlinear weights for any point in a cell [15]. They differ from the classical WENO in that the sectorial polynomials may have a smaller degree. Thus their stencil can be chosen inside the stencil of the central optimal polynomial [15]. This reconstruction procedure reduces the size of the directional stencils and, consequently, approximation from them. This simplicity offers a reduced computational cost and is less complicated than the traditional WENO. The increased compactness of this class of schemes makes them more suitable to be deployed for frameworks such as DG, as seen in [16]. However, one of the most overlooked benefits is the robustness of these types of CWENO schemes since the reduced size of the directional stencils translates to a higher probability of at least one of them lying in a region with a smooth variation of data compared to the traditional WENO schemes for unstructured meshes.

In this article, the CWENO will be used to simulate viscous compressible multicomponent flow problems to test its advantages in the interface-capturing method's finite-volume framework using the five equations proposed by Allaire et al. [3]and Kapila et al. [2].

All the schemes are developed in the open-source UCNS3D solver [17]. We assess their performance in terms of robustness, accuracy and computational efficiency for two test problems while comparing them with other high-order schemes. The paper is organized as follows: Section

2 introduces the governing equations that describe the five-equation diffused interface models and the CWENO schemes' reconstruction process while describing the chosen fluxes and temporal discretisation employed. Section 3 presents the two test cases and their numerical results obtained and compared against analytical and reference solutions whenever possible. Finally, the last section describes the conclusions drawn from this study.

2 THE GOVERNING EQUATIONS.

2.1 The five-equations diffuse-interface model of Allaire et al.

The five-equations models are often referred to as the mechanical equilibrium models, i.e. we assume that the momentum, energy, and mass transfer between the phases reach equilibrium due to the thermodynamic difference between each component. The equations are presented below:

$$\frac{\partial(\alpha_1\rho_1)}{\partial t} + \nabla\cdot(\alpha_1\rho_1\mathbf{v}) = 0, \tag{1}$$

$$\frac{\partial(\alpha_2\rho_2)}{\partial t} + \nabla\cdot(\alpha_2\rho_2\mathbf{v}) = 0, \tag{2}$$

$$\frac{\partial\rho\mathbf{v}}{\partial t} + \nabla\cdot(\rho\mathbf{v}\mathbf{v} + p\mathbf{I}) = 0, \tag{3}$$

$$\frac{\partial E}{\partial t} + \nabla\cdot(E+p)\mathbf{v} = 0, \tag{4}$$

$$\frac{\partial\alpha_1}{\partial t} + \mathbf{v}\cdot\nabla\alpha_1 = 0, \tag{5}$$

where the subscript 1, 2 represents gas or liquid phase, respectively, ρ is the density, v = (u, v, w) is the velocity, p is the pressure, E is the total energy and α is the volume fraction of each component.

The total density, momentum, kinetic and internal energy of the mixture is stated below:

$$\begin{cases} \rho = \sum_{i=1}^{N}\alpha_i\rho_i & : \text{ total density of the mixture.} \\ \rho\vec{V} = \sum_{i=1}^{N}\alpha_i\left(\rho_i\vec{v}\right) & : \text{ momentum of the mixture.} \\ \rho e^{\mathrm{K}} = \sum_{i=1}^{N}\alpha_i\rho_i e_i^{\mathrm{K}} & : \text{ mixture kinetic energy.} \\ \rho e^{\mathrm{I}} = \sum_{i=1}^{N}\alpha_i\rho_i e_i^{\mathrm{I}} & : \text{ mixture internal energy.} \end{cases} \tag{6}$$

So the total energy can be expressed as:

$$\sum_{i=1}^{N}\rho e^{\mathrm{T}} = \sum_{i=1}^{N}(\alpha_i\left(\rho_i e_i^{\mathrm{I}}\right) + \frac{\rho_i.V^2}{2})) \tag{7}$$

To determine the internal energy and put closure to the equations, it is convenient to use the stiffened the EOS for both fluid component:

$$P_i = (\gamma_i - 1)\,\rho_i e_i - \gamma_i P_{c,i} \tag{8}$$

the internal energy $\rho_i e_i$ can now be expressed as:

$$\frac{p + \gamma_i.P_c, i}{\gamma_i - 1} \tag{9}$$

and the total energy below:

$$\sum_{i=1}^{N} \alpha_i (\frac{p + \gamma_i.P_c, i}{\gamma_i - 1} + \frac{\rho_i.V^2}{2}) \tag{10}$$

The five-equations diffused interface model can be expressed into the following general form of a non-linear system of PDE in multiple space dimensions:

$$\frac{\partial \mathbf{Q}}{\partial t} + \nabla \cdot \mathbf{F}(\mathbf{Q}) + \mathbf{H}(\mathbf{Q}) \nabla \cdot U = \mathbf{S}(\mathbf{Q}) \tag{11}$$

Where Q is the vector of evolution variables (conserved and not conserved), F is a flux function, U is the velocity field, and H and S are non-conservative quantities.

In a matrix form, the 5-equations model is presented below:

$$Q = \begin{bmatrix} \alpha_1\rho_1 \\ \alpha_2\rho_2 \\ \rho u \\ E \\ \alpha_1 \end{bmatrix}, \quad F = \begin{bmatrix} \alpha_1\rho_1 u \\ \alpha_2\rho_2 u \\ \rho u^2 + P \\ u(E+P) \\ \alpha_1 u \end{bmatrix}, \quad H1 = \begin{bmatrix} 0 \\ 0 \\ 0 \\ 0 \\ -\alpha_1 \end{bmatrix} \text{(Allaire et al.)}, H2 = \begin{bmatrix} 0 \\ 0 \\ 0 \\ 0 \\ -\alpha_1 - k \end{bmatrix} \text{(Kapila et al.)}, \tag{12}$$

The k function in the H non-conservative quantity differentiates Kapila's model et al. from the Allaire's et al.The k function in Kapila's et al. can be determined from the equation 13 where the mixture's speed of sound is gotten using the wood's speed of sound as seen in equation 14.

$$k = \alpha_1\alpha_2 \left(\frac{1}{\rho_1 c_1^2} - \frac{1}{\rho_2 c_2^2} \right) \rho c^2 \tag{13}$$

where c_1 and c_2 is given as :

$$c_1 = \sqrt{\frac{\gamma_1}{\rho_1}(p + p_{c,1})}, c_2 = \sqrt{\frac{\gamma_2}{\rho_2}(p + p_{c,2})} \tag{14}$$

and the mixture speed of sound is given as:

$$\frac{1}{\rho c^2} = \frac{\alpha_1}{\rho_1 c_1^2} + \frac{\alpha_2}{\rho_2 c_2^2} = \sum_{i=1}^{N} \frac{\alpha_i}{\rho_i c_i^2} \tag{15}$$

The non-conservative advection equation of the volume fraction in equation 5 is simplified using Johnsen and Colonius [9] approach to obtain a quasi-conservative form:

For Allaire's et al.

$$\frac{\partial \alpha_1}{\partial t} + \nabla \cdot f = (\alpha_1)\, \nabla \cdot V \tag{16}$$

For Kapila's et al.

$$\frac{\partial \alpha_1}{\partial t} + \nabla \cdot f = (\alpha_1 + K)\, \nabla \cdot V \tag{17}$$

The K$\nabla\cdot$ u terms in Kapila's model describe the thermodynamic properties (expansion and compression of each phase) of the mixture region of the two-phase fluid [18].

3 NUMERICAL METHOD

3.1 Spatial Disretisation

Consider a 3D domain Ω consisting of conforming tetrahedral, hexahedral, prism, and pyramid cells each one of them indexed by a unique mono-index i, and the governing equations of the five-equation model written in vector form as follows:

$$\frac{\partial}{\partial t} \int_{V_i} \mathbf{U}\, dV + \int_{\partial V_i} \mathbf{F}_n\, dS = \int_{V_i} \mathbf{s}\, dV \tag{18}$$

where $\mathbf{U} = \mathbf{U}(\mathbf{x}, t)$ is the vector of conserved variables and the volume fraction of one species, $\mathbf{F}_n$ is the non-linear flux in the direction normal to the cells interface as given below:

$$\mathbf{U} = \begin{bmatrix} a_1\rho_1 \\ a_2\rho_2 \\ \rho u \\ \rho v \\ \rho w \\ E \\ a_1 \end{bmatrix}, \mathbf{F}_n = \begin{bmatrix} a_1\rho_1 u_n \\ a_2\rho_2 u_n \\ \rho u u_n + n_x p \\ \rho v u_n + n_y p \\ \rho w u_n + n_z p \\ u_n(E+p) \\ a_1 u_n \end{bmatrix}, \tag{19}$$

where u_n is the velocity normal to the bounded surface area, defined by $u_n = n_x u + n_y v + n_z w$. The source term $\mathbf{s}$ is with regards to the term $a_1 \nabla \cdot \mathbf{u}$ of Eq. (5). Following the approach of Johnsen and Colonius [**?**] the source term is numerically approximated as surface integral, rather than a volume one, while using the same velocity estimate as the one used for the evaluation of the fluxes as shown below:

$$\int_{V_i} a_1 \nabla \cdot \mathbf{u}\, dV \approx \int_{V_i} a_1\, dV \cdot \int_{\partial V_i} (u_n)^{Riem.}\, dS. \tag{20}$$

Integrating Eq. (18) over the mesh element i using a high-order explicit finite-volume formulation the following equation is obtained that incorporates the source term as previously defined:

$$\frac{d\mathbf{U}_i}{dt} = \frac{1}{|V_i|}\sum_{j=1}^{N_f}\sum_{\alpha=1}^{N_{qp}}\left(F_{\mathbf{n_{ij}}}\left(\mathbf{U}^n_{ij,L}(\mathbf{x}_{ij,\alpha},t),\mathbf{U}^n_{ij,R}(\mathbf{x}_{ij,\alpha},t)\right) - \mathbf{a}^n_{i,1}\cdot u_n^{Riem}(\mathbf{x}_{ij,\alpha},t)\right)\omega_\alpha|S_{ij}|, \quad (21)$$

where $\mathbf{U}_i$ is the volume averaged vector of variables

$$\mathbf{U}_i = \frac{1}{|V_i|}\int_{V_i}\mathbf{U}(x,y,z)\,dV, \quad (22)$$

and $F_{\mathbf{n_{ij}}}$ is a numerical flux function in the direction normal to the cell interface between a considered cell i and one of its neighbouring cells j. N_f is the number of faces per element, N_{qp} is the number of quadrature points used for approximating the surface integrals, $|S_{ij}|$ is the surface area of the corresponding face, and $\mathbf{U}^n_{ij,L}(\mathbf{x}_{ij,\alpha},t)$ and $\mathbf{U}^n_{ij,R}(\mathbf{x}_{ij,\alpha},t)$ are the high-order approximations of the solutions for cell i and cell j respectively. α corresponds to different Gaussian integration points $\mathbf{x}_\alpha$ and weights ω_α over each face. $\mathbf{a}^n_{i,1}$ corresponds to the volume averaged volume fraction of cell i at time level n. The volume, surface and line integrals are numerically approximated by a suitable Gauss-Legendre quadrature.

The reconstruction process adopted in `ucns3d` [17, 19] follows the approaches of Tsoutsanis et al. [20–23], Titarev et al. [24] that have been previously applied to smooth and discontinuous flow problems [17, 20–41].

3.2 CWENO high-order schemes

The CWENO scheme employed in this study follows the implementation of Tsoutsanis and Dumbser [23]. It is the combination of an optimal (high-order) polynomial p_{opt} with lower-order polynomials. The optimal polynomial uses the central stencil, while the lower-order polynomials employ the directional stencils. When the variation of the solution is smooth, the optimal polynomial is recovered and therefore, the desired order of accuracy is obtained, whereas at the presence of discontinuous data, at least one of the lower-order polynomials arising from the directional stencils could contain smooth data, hence essentially reducing the oscillations in the computed solution. All the polynomials involved satisfying the requirement of matching the cell averages of the solution. Therefore they are solved with the same constrained least-squares technique. The directional stencils employ the Type3 definition which includes one directional stencil per element face as detailed in the work by Tsoutsanis [40]. The optimal polynomial is defined as follows:

$$p_{opt}(\xi,\eta,\zeta) = \sum_{s=1}^{s_t}\lambda_s p_s(\xi,\eta,\zeta), \quad (23)$$

where s is the stencil index, with $c = 1$ being the central, $c = 2, 3, .$ being the directional, s_t being the total number of stencils, and λ_s being the linear coefficients for each stencil, whose sum is equal to 1. The p_1 polynomial is not computed directly but computed by subtracting the lower-order polynomials from the optimum polynomial as follows:

$$p_1(\xi,\eta,\zeta) = \frac{1}{\lambda_1}\left(p_{opt}(\xi,\eta,\zeta) - \sum_{s=2}^{s_t}\lambda_s p_s(\xi,\eta,\zeta)\right). \quad (24)$$

The CWENO reconstruction polynomial is given as a non-linear combination of all the polynomials in the following manner:

$$p(\xi,\eta,\zeta)^{\text{cweno}} = \sum_{s=1}^{s_t} \omega_s p_s(\xi,\eta,\zeta), \tag{25}$$

where ω_s correspond to the nonlinear weights assigned to each polynomial, and in regions with smooth data $\omega_s \approx \lambda_s$, hence obtaining the high-order approximation from the central stencil, and in regions of discontinuous solutions the reconstructed solution will be mostly influenced from the lower-order polynomials of the directional stencils. where $\tilde{a}_k$ are the reconstructed degrees of freedom; and the non-linear weight ω_s is defined as:

$$\omega_s = \frac{\tilde{\omega}_s}{\sum_{s=1}^{s_t} \tilde{\omega}_s} \quad \text{where} \quad \tilde{\omega}_s = \frac{\lambda_m}{(\epsilon + \mathcal{SI}_s)^b}. \tag{26}$$

The smoothness indicator $\mathcal{SI}_m$ is given by:

$$\mathcal{SI}_s = \sum_{1\leq|\beta|\leq r} \int_{V_0'} \left(\mathcal{D}^\beta p_s(\xi,\eta,\zeta)\right)^2 (d\xi, d\eta, d\zeta), \tag{27}$$

where β is a multi-index, r is the polynomial's order, λ_m is the linear weight. The value set to prevent division by zero of $\epsilon = 10^{-6}$ is used, with $b = 4$ and $\mathcal{D}$ being the derivative operator. The smoothness indicator is a quadratic function of the degrees of freedom (a_k^s) and Eq. (27) can be rewritten as:

$$\mathcal{SI}_s = \sum_{k=1}^{K} a_k^s \left(\sum_{q=1}^{K} \mathcal{OI}_{kq} a_q^s \right), \tag{28}$$

where the oscillation indication matrix $\mathcal{OI}_{kq}$ is given by:

$$\mathcal{OI}_{kq} = \sum_{1\leq|\beta|\leq r} \int_{V_0'} \left(\mathcal{D}^\beta \phi_k(\xi,\eta,\zeta)\right) \left(\mathcal{D}^\beta \phi_q(\xi,\eta,\zeta)\right) (d\xi, d\eta, d\zeta), \tag{29}$$

which can be precomputed and stored at the beginning of the simulation. We employ $r = 1$ to obtain 2nd-order accuracy and any arbitrary order of accuracy for the polynomial associated with the central stencil for the directional stencils and their corresponding polynomials. The linear weights are computed by firstly assigning the non-normalised linear weight for the central stencil $\lambda_1^{'}$ an arbitrary value, and then normalising this as follows:

$$\lambda_1 = 1 - \frac{1}{\lambda_1^{'}}, \tag{30}$$

with the linear weights associated with lower-order polynomials being equal and provided by the following expression:

$$\lambda_s = \frac{1-\lambda_1}{s_t - 1}, \tag{31}$$

where s_t is the total number of stencils. From this point forward the order of the scheme will be defined by a number next to the type of the scheme, such as CWENO3 and WENO4 corresponding to a 3rd-order CWENO scheme and a 4th-order WENO scheme, respectively [23].

4 TEST CASES

Using the high order CWENO in conjunction with the 5-equation interface capturing schemes models, two test problems were selected to test the proposed algorithm.

4.1 Advection of contact discontinuity

The advection test problem is frequently used for verification of the numerical accuracy, such as the non-oscillatory properties and convergence of their proposed numerical scheme. Among notables works are [8–10,42]. This multispecies test case describes the advection of an interface of two inert gases; Nitrogen Ni and Helium He, respectively. The specific heat capacity of the gases are 1.66 and 1.4, and the right side is the gas-Ni while the left side is the gas He. The temperature, pressure and velocity of both components are constant across the material interface. The results are accurate when the velocity, pressure, and temperature are maintained at equilibrium. The robustness of the numerical framework for multiphase and multicomponent flow will be tested using the traditional WENO and our CWENO high order schemes on unstructured meshes for the 5-equation diffuse-interface multicomponent models of Allaire et al [3].

Using the initial data of Wong et al. [42], the computational domain is a square domain ϵ [1.0m x 1.0m] and discretized using an hybrid unstructured mesh of triangular and quadrilateral mesh elements of 80 edges per side resolution. The final time of the simulation is selected as t= 2ms with a CFL number of 0.6 and evolved with a constant time step of $\Delta t = 0.005$. .
The initial physical parameters of each fluid:

$$(\rho, u, v, p, \gamma, \alpha) = \begin{cases} (Ni : 10.0, 0.5, 0, 1/1.4, 1.4, 1)\,, & 0.25 \leq\ x <\ 0.75 \\ (He : 1.0, 0.5, 0, 1/1.4, 1.66, 0)\,, & x < 0.25\ or\ x \geq\ 0.75 \end{cases} \tag{32}$$

Using the HLLC Riemann solver to upwind the fluxes, reconstruction is done using primitive variables in the classical WENO schemes and also the CWENO schemes. Using the third-order WENO and CWENO schemes, results obtained for this gas-gas advection problem in density, temperature, pressure and velocity are shown in Fig. 1.The results show the CWENO method has better computational efficiency while maintaining it's ability to avoid spurious oscillations in the areas of contact discontinuities as compared to the traditional or classical WENO schemes of the same order of accuracy for the same mesh size and type. In terms of computational resources, the CWENO gives a reduced computational cost (Table 2) at about four times faster than the corresponding WENO schemes, respectively, for the same grid size. This is explained as written in the paper by Dumbser [43], the fact that the CWENO employs one single set of linear weights and thus means that the output of the CWENO reconstruction is not given by some point values like the WENO schemes from several stencils significantly makes WENO more expensive for the same grid. These simple but substantial changes leaves the CWENO schemes a better choice for multiphase/multicomponent compressible flow.

In Fig. 2, we compare the results obtained for CWENO schemes(from third to sixth order of accuracy) on the same plot and the exact solution using plots for density, the temperature and the volume fraction. The relative error for the pressure and u-velocity variable is measured and plotted in 2. It can be seen that both the velocity and pressure errors are close to machine precision for all of the order of accuracy. The error in the pressure is in the range of $[10^{-13}]$

while that of the velocity-u and v profile contains an error in the range of $[10^{-15}]$.

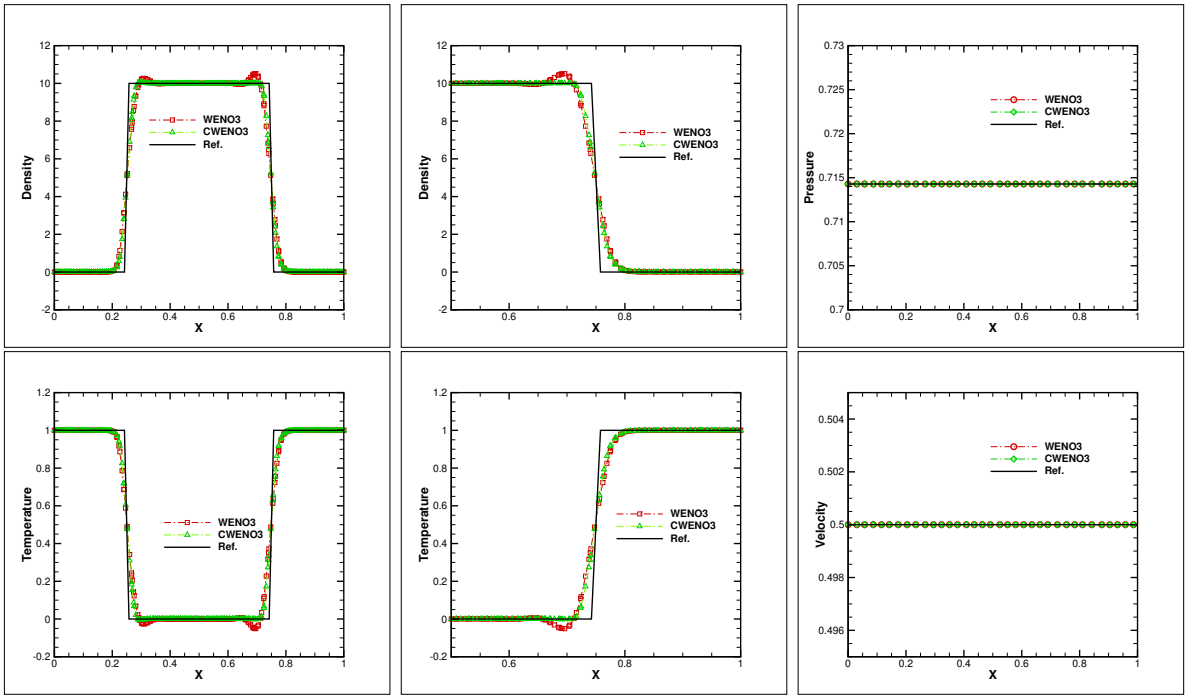

Figure 1: Advection of a material interface; the solid line is the exact solution;Plots of density and temperature at t = 2 obtained with CWENO3 and WENO3 schemes using primitive variables reconstructions shows that the the WENO3 produces oscillations near the material interface, while they are absent from the CWENO3. reconstruction.

Table 1 shows the Normalised Computational time using both WENO and CWENO schemes.

	CWENO				WENO			
Order	3rd	4th	5th	6th	3rd	4th	5th	6th
Time	1.00	1.41-	1.85	2.28	3.61	4.95	7.00	9.39

4.2 Underwater explosion near a free surface

We consider another multiphase/multicomponent test problem involving cavitation to test the numerical algorithm for flows involving cavitation. Various authors have studied this work numerically and used it to validate their numerical algorithms [10, 44–46]. Using the initial data of Shukla et al. [46], the computational domain is a square area $[\,2,\,2\,] \times [\,1\,.\,5,\,2\,.\,5\,]$. A

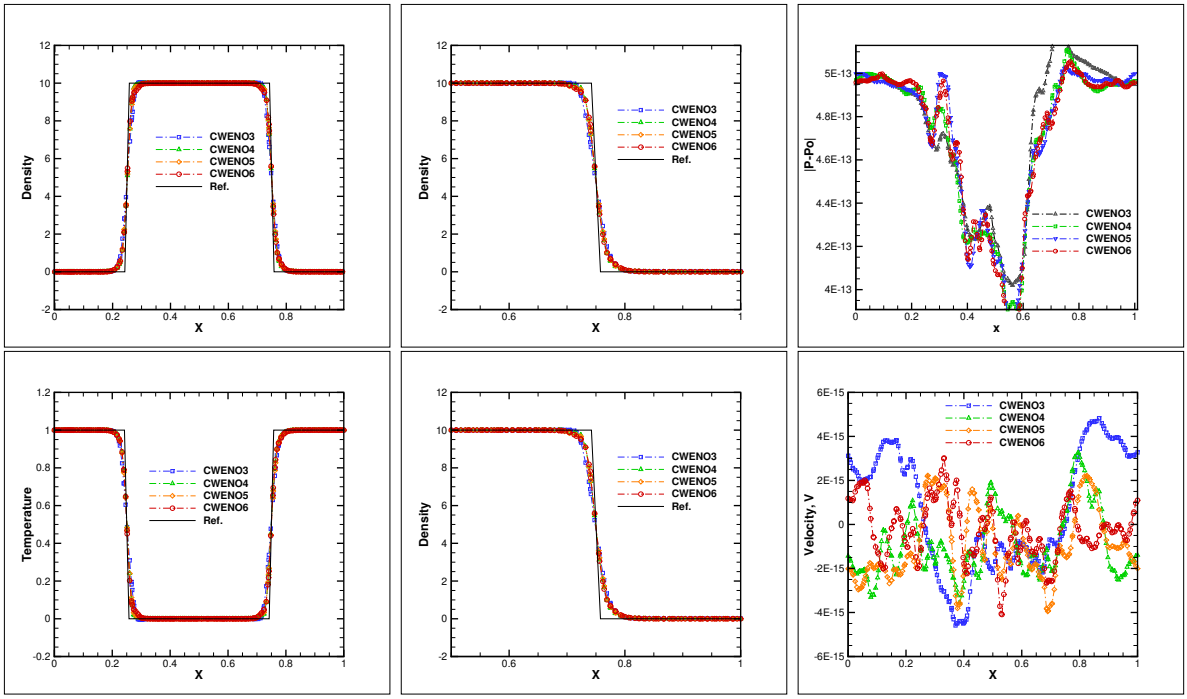

Figure 2: Temperature and density profile for the CWENO schemes third up to sixth order of accuracy, the solid line is the exact solution. The bottom plot shows the errors in isolated material interface problem at t= 2 using CWENO schemes for accuracy order from third to sixth in the pressure and velocity profile where it can be seen that the minute oscillations are close to machine precision.

high-pressure gas bubble of a diameter of 0.24 is placed at [0, -0.3]of the two-phase medium with air-water interface positioned at the centre of the computational domain. The boundary conditions of the lower surface are set up as reflecting, the lateral surfaces and the upper surface as transparent boundary conditions. The final time of the simulation is selected as t= 1.2ms. The initial physical parameters of each fluid are given as:

$$\rho, u, v, p, \gamma\, \alpha) = \begin{cases} \left(1.225, 0, 0, 10^5, 2.0, 0\right), & \text{Air} \\ \left(1250, , 0, 0, 10^9, 2.0, 1\right), & \text{Explosive} \\ \left(1000, 0, 0, 10^5, 7.15, 0\right), & \text{Water.} \end{cases} \tag{33}$$

As the air bubble explodes and evolves from a spherical shape into an oval formation, numerical Schlieren obtained for density gradient in Fig. 4 shows that the CWENO4 is able to capture the interfacial region between the bubble and the air-water medium with less smearing or numerical diffusion without using interface sharpening [46] or anti-diffusion technique [47] used by most authors to improve their results. As seen in in Fig. 3, for a similar mesh, the result obtained in the form of a density plot at different instants (t=0.4ms and 0.8ms) shows good agreement with the published result [47] where the anti-diffusion technique is used. The use of interface sharpening or anti-diffusion technique often leads to a loss of discrete conservation,

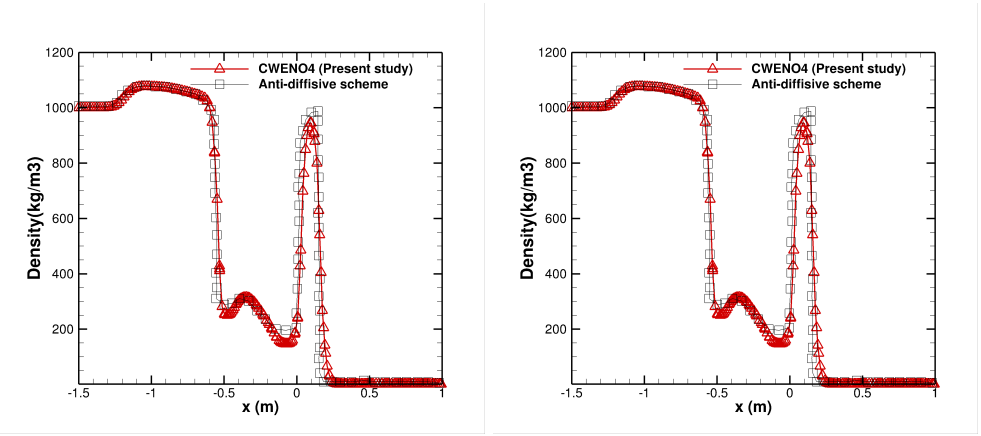

Figure 3: Density plot along horizontal axis x=0 for underwater explosion with free surface at instants t= (0.4; 0.8)ms. Comparison are made with the results of Kokh et al [47].

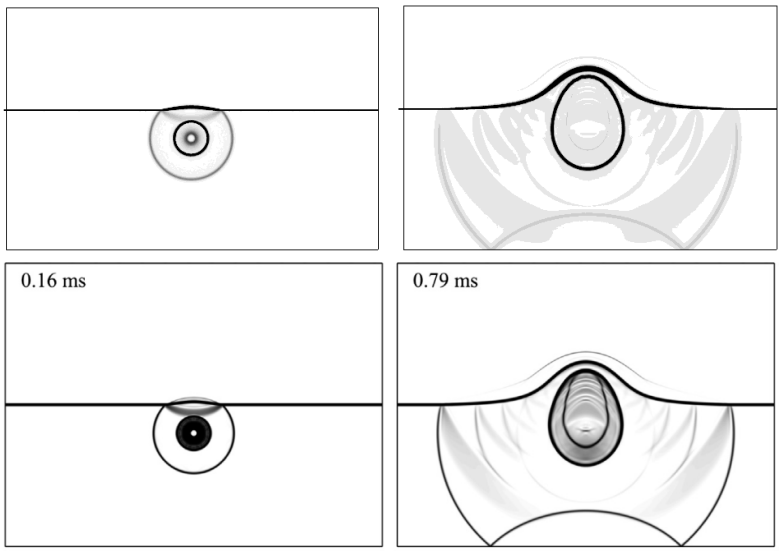

Figure 4: Schlieren images of density gradient using a CWENO4 scheme(top) on a fine mesh at t=0.16ms and 0.79ms in comparison with the images obtained by numerical studies of Shukla et al. [48]in which an additional interface sharpening technique is used on similar grid to ensure that the thickness of the artificial diffuse zone is kept to a minimum.

which many authors choose to forgo in favour of improved accuracy. The CWENO result can give a good result without the challenge mentioned earlier.

5 CONCLUSIONS

The results from this paper demonstrate that the CWENO schemes can achieve high-order accurate solutions in smooth regions while providing oscillation free solutions. They do that

while exhibiting less numerical dissipation in comparison with existing high-order methods and they provide a sharp description of the moving material interface with less numerical smearing. Resorting to additional interface sharpening or interface compression technique could be explored in the future in particular for up to 3rd-order methods where there is sufficient evidence in the literature to support that these methods can benefit significantly.

REFERENCES

[1] R. Saurel, C. Pantano, Diffuse-interface capturing methods for compressible two-phase flows richard, The Annual Review of Fluid Mechanics 50 (2018) 105–30. doi:10.1146/annurev-fluid-122316-050109.

[2] A. Kapila, R. Menikoff, B. J.B., S. Son, D. S. Stewart, Two-phase modeling of deflagration-to-detonation transition in granular materials: reduced equations, Physics of Fluids 13 (2001) 3002–3024.

[3] G. Allaire, S. Clerc, S. Kokh, A five-equation model for the simulation of interfaces between compressible fluids, Journal of Computational Physics 181 (2) (2002) 577–616. doi:https://doi.org/10.1006/jcph.2002.7143.

[4] R. Saurel, F. Petitpas, B. R.A., Simple and efficient relaxation methods for interfaces separating compressible fluids, cavitating flows and shocks in multiphase mixtures, Journal of Computational Physics 228 (2009) 1678–1712.

[5] A. Murrone, H. Guillard, A five equation reduced model for compressible two phase flow problems, Journal of Computational Physics 202 (2) (2005) 664–698. doi:10.1016/j.jcp.2004.07.019.

[6] E. Romenski, Multiphase flow modeling based on the hyperbolic thermodynamically compatible systems theory, AIP Conference Proceedings 1648 (November) (2015). doi:10.1063/1.4912321.

[7] V. Maltsev, M. Skote, P. Tsoutsanis, High-order methods for diffuse-interface models in compressible multi-medium flows: A review, Physics of Fluids 34 (2) (2022). doi:10.1063/5.0077314.

[8] M. Ansari, A. Daramizadeh, Numerical simulation of compressible two-phase flow using a diffuse interface method, International Journal of Heat and Fluid Flow 42 (2013) 209–223. doi:10.1016/j.ijheatfluidflow.2013.02.003.

[9] J. E., C. T., Implementation of weno schemes in compressible multicomponent flow problems, Journal of Computational Physics 219 (2) (2006) 715–732. doi:10.1016/j.jcp.2006.04.018.

[10] Numerical simulations of compressible multicomponent and multiphase flow using a high-order targeted ENO (TENO) finite-volume method, Computers and Fluids 146 (2017) 105–116. doi:10.1016/j.compfluid.2017.01.012.
URL http://dx.doi.org/10.1016/j.compfluid.2017.01.012

[11] E. M. Henry de Frahan, S.Varadan, A new limiting procedure for discontinuous Galerkin methods applied to compressible multiphase flows with shocks and interfaces, Journal of Computational Physics 280 (2015) 489–509. doi:https://doi.org/10.1016/j.jcp.2014.09.030.
URL http://www.sciencedirect.com/science/article/pii/S0021999114006664

[12] Q. Wang, R. Deiterding, J. Pan, Y. X. Ren, Consistent high resolution interface-capturing finite volume method for compressible multi-material flows, Computers and Fluids 202 (2020). doi:10.1016/j.compfluid.2020.104518.

[13] V. Coralic, T. Colonius, Finite-volume WENO scheme for viscous compressible multicomponent flows, Journal of Computational Physics 274 (2014) 95–121. doi:10.1016/j.jcp.2014.06.003.
URL http://dx.doi.org/10.1016/j.jcp.2014.06.003

[14] J. Cheng, C. Shu, High Order Schemes for CFD: A Review, Chinese Journal of Computational Physics 26 (2009) 1–50.

[15] M. Dumbser, W. Boscheri, M. Semplice, G. Russo, Central Weighted ENO Schemes for Hyperbolic Conservation Laws on Fixed and Moving Unstructured Meshes, SIAM J. Sci. Comput. 39 (2017).

[16] H. Zhu, J. Qiu, J. Zhu, A simple, high-order and compact WENO limiter for RKDG method, Computers & Mathematics with Applications 79 (2) (2020) 317–336. doi:https://doi.org/10.1016/j.camwa.2019.06.034.

[17] UCNS3D CFD code, http://www.ucns3d.com, accessed: 2022-05-05.

[18] T. K. Schmidmayer, S.H. Bryngelson, An assessment of multicomponent flow models and interface capturing schemes for spherical bubble dynamics 402 (2020) 209–223. doi:https://doi.org/10.1016/j.jcp.2019.109080,.

[19] A. F. Antoniadis, D. Drikakis, P. S. Farmakis, L. Fu, I. Kokkinakis, X. Nogueira, P. A. Silva, M. Skote, V. Titarev, P. Tsoutsanis, Ucns3d: An open-source high-order finite-volume unstructured cfd solver, Computer Physics Communications 279 (2022) 108453. doi:https://doi.org/10.1016/j.cpc.2022.108453.
URL https://www.sciencedirect.com/science/article/pii/S0010465522001722

[20] P. Tsoutsanis, V. Titarev, D. Drikakis, WENO schemes on arbitrary mixed-element unstructured meshes in three space dimensions, Journal of Computational Physics 230 (4) (2011) 1585–1601.

[21] P. Tsoutsanis, A. Antoniadis, D. Drikakis, WENO schemes on arbitrary unstructured meshes for laminar, transitional and turbulent flows, Journal of Computational Physics 256 (2014) 254–276.

[22] P. Tsoutsanis, M. Dumbser, Arbitrary high order central non-oscillatory schemes on mixed-element unstructured meshes, Computer and Fluids 225 (2021). doi:10.1016/j.compfluid.2021.104961.

[23] P. Tsoutsanis, E. M. Adebayo, A. Carriba Merino, A. Perez Arjona, M. Skote, CWENO finite-volume interface capturing schemes for multicomponent flows using unstructured meshes, Journal of Scientific Computing 89 (2021). doi:10.1007/s10915-021-01673-y.

[24] V. Titarev, P. Tsoutsanis, D. Drikakis, WENO schemes for mixed-element unstructured meshes, Communications in Computational Physics 8 (3) (2010) 585–609.

[25] P. Tsoutsanis, D. Drikakis, A high-order finite-volume method for atmospheric flows on unstructured grids, Journal of Coupled Systems and Multiscale Dynamics 4 (2016) 170–186. doi:10.1166/jcsmd.2016.1104.

[26] A. Antoniadis, P. Tsoutsanis, D. Drikakis, Numerical accuracy in RANS computations of high-lift multi-element airfoil and aircraft configurations, in: 53rd AIAA Aerospace Sciences Meeting, Vol. 0317, 2015. doi:10.2514/6.2015-0317.

[27] A. Antoniadis, P. Tsoutsanis, D. Drikakis, High-order schemes on mixed-element unstructured grids for aerodynamic flows, in: 42nd AIAA Fluid Dynamics Conference and Exhibit, Vol. 2833, 2012. doi:10.2514/6.2012-2833.

[28] A. Antoniadis, P. Tsoutsanis, I. Kokkinakis, Z. Rana, D. Drikakis, Azure: An advanced CFD software suite based on high-resolution and high-order methods, in: 53rd AIAA Aerospace Sciences Meeting, Vol. 0813, 2015. doi:10.2514/6.2015-0813.

[29] A. Antoniadis, D. Drikakis, I. W. Kokkinakis, P. Tsoutsanis, Z. Rana, High-order methods for hypersonic shock wave turbulent boundary layer interaction flow, in: 20th AIAA International Space Planes and Hypersonic Systems and Technologies Conference, Vol. 3524, 2015. doi:10.2514/6.2015-3524.

[30] P. Tsoutsanis, I. Kokkinakis, L. Konozsy, D. Drikakis, R. Williams, D. Youngs, Comparison of structured- and unstructured-grid, compressible and incompressible methods using the vortex pairing problem, Computer Methods in Applied Mechanics and Engineering 293 (2015) 207–231. doi:10.1016/j.cma.2015.04.010.

[31] P. Tsoutsanis, H. Srinivasan, Adaptive mesh refinement techniques for high-order finite-volume WENO schemes, in: ECCOMAS Congress 2016, Crete, Greece, 2016. doi:10.7712/100016.2003.8544.

[32] P. Tsoutsanis, N. Simmonds, A. Gaylard, Implementation of a low-Mach number modification for high-order finite-volume schemes for arbitrary hybrid unstructured meshes, in: ECCOMAS Congress 2016, Crete, Greece, 2016. doi:10.7712/100016.2004.8545.

[33] P. Tsoutsanis, D. Drikakis, Addressing the challenges of implementation of high-order finite-volume schemes for atmospheric dynamics on unstructured meshes, in: ECCOMAS Congress 2016, Crete, Greece, 2016. doi:10.7712/100016.1846.8406.

[34] P. Tsoutsanis, A. Antoniadis, K. Jenkins, Improvement of the computational performance of a parallel unstructured WENO finite volume CFD code for implicit large eddy simulation, Computers and Fluids 173 (2018) 157–170. doi:10.1016/j.compfluid.2018.03.012.

[35] P. Farmakis, P. Tsoutsanis, X. Nogueira, WENO schemes on unstructured meshes using a relaxed a posteriori MOOD limiting approach, Computer Methods in Applied Mechanics and Engineering 363 (2020). doi:10.1016/j.cma.2020.112921.

[36] P. Tsoutsanis, Extended bounds limiter for high-order finite-volume schemes on unstructured meshes, Journal of Computational Physics 362 (2018) 69–94.

[37] N. Simmonds, P. Tsoutsanis, A. Antoniadis, K. Jenkins, A. Gaylard, Low-Mach number treatment for finite-volume schemes on unstructured meshes, Applied Mathematics and Computation 336 (2018) 368–393.

[38] F. Ricci, P. Silva, P. Tsoutsanis, A. Antoniadis, Hovering rotor solutions by high-order methods on unstructured grids, Aerospace Science and Technology 97 (2020). doi:10.1016/j.ast.2019.105648.

[39] P. Silva, P. Tsoutsanis, A. Antoniadis, Simple multiple reference frame for high-order solution of hovering rotors with and without ground effect, Aerospace Science and Technology 111 (2021). doi:10.1016/j.ast.2021.106518.

[40] P. Tsoutsanis, Stencil selection algorithms for WENO schemes on unstructured meshes, Journal of Computational Physics: X 4 (2019). doi:10.1016/j.jcpx.2019.100037.

[41] A. F. Antoniadis, P. Tsoutsanis, D. Drikakis, Assessment of high-order finite volume methods on unstructured meshes for rans solutions of aeronautical configurations, Computers and Fluids 146 (2017) 86–104. doi:https://doi.org/10.1016/j.compfluid.2017.01.002.

[42] M. L. Wong, S. K. Lele, High-order localized dissipation weighted compact nonlinear scheme for shock- and interface-capturing in compressible flows, Journal of Computational Physics 339 (March) (2017) 179–209. arXiv:1701.08905, doi:10.1016/j.jcp.2017.03.008.
URL `http://dx.doi.org/10.1016/j.jcp.2017.03.008`

[43] M. Dumbser, W. Boscheri, M. Semplice, G. Russo, Central weighted eno schemes for hyperbolic conservation laws on fixed and moving unstructured meshes, SIAM Journal on Scientific Computing 39 (6) (2017) A2564–A2591. doi:10.1137/17M1111036.

[44] N. V. Petrov, A. A. Schmidt, Multiphase phenomena in underwater explosion, Experimental Thermal and Fluid Science 60 (May) (2015) 367–373. doi:10.1016/j.expthermflusci.2014.05.008.

[45] Numerical simulation of underwater explosion near air-water free surface using a five-equation reduced model, Ocean Engineering 110 (2015) 25–35. doi:10.1016/j.oceaneng.2015.10.003.
URL `http://dx.doi.org/10.1016/j.oceaneng.2015.10.003`

[46] R. K. Shukla, Nonlinear preconditioning for efficient and accurate interface capturing in simulation of multicomponent compressible flows, Journal of Computational Physics 276 (2014) 508–540. doi:10.1016/j.jcp.2014.07.034.
URL `http://dx.doi.org/10.1016/j.jcp.2014.07.034`

[47] S. Kokh, F. Lagoutière, An anti-diffusive numerical scheme for the simulation of interfaces between compressible fluids by means of a five-equation model, Journal of Computational Physics 229 (8) (2010) 2773–2809. doi:10.1016/j.jcp.2009.12.003.
URL http://dx.doi.org/10.1016/j.jcp.2009.12.003

[48] R. K. Shukla, Nonlinear preconditioning for efficient and accurate interface capturing in simulation of multicomponent compressible flows, Journal of Computational Physics 276 (3) (2014) 508–540. doi:10.1016/j.jcp.2014.07.034.